



Temperature measurement of the reaction zone during polyamide film formation by interfacial polymerization

Ben Ukrainsky, Guy Z. Ramon*

Department of Civil and Environmental Engineering, Technion – Israel Institute of Technology, Haifa 32000, Israel



ABSTRACT

Composite membranes used for water purification are formed by interfacial polymerization (IP), where choices of chemistry, formulation and reaction conditions conspire to dictate the final membrane performance. Here, we report in-situ visualization experiments of IP, performed using a microfluidic platform, under several representative conditions. Calibrated, temperature-sensitive fluorescence intensity enabled mapping of microscopic fluorescent images into temperature fields. Specifically, the temperature at the interface was monitored and illustrated a two-stage time-evolution, increasing rapidly at early times and then tapering. Polymerization appears to proceed so long as monomers are supplied, suggesting that the process may not be truly self-limiting. Results further show that under conditions promoting fast mass transfer and supply of monomers, temperatures at the interface may reach the boiling point of some solvents. Such interfacial boiling or release of dissolved gasses may be responsible for the formation of voids recently shown to exist in polyamide thin films. Curiously, the morphologies formed in the microfluidic experiments resemble commercial membranes despite the disparate length-scales involved, suggesting a possible spatial similitude. Ultimately, extensions beyond our current device, adding the capability to measure transport properties of the film formed within the device, can lead to a microfluidic-based platform to be used for rapid prototyping of materials, using small samples and short time scales, and provide insight for better informed membrane design.

1. Introduction

State-of-the-art membranes used for water purification - Reverse Osmosis (RO) and Nanofiltration - are thin-film composites (TFC) comprised of a porous support and an ultra-thin 'active layer', formed on top of it [1]. This layer is created using interfacial polymerization (IP) between two monomers at the interface formed between two immiscible fluids: an aqueous phase containing a polyfunctional amine monomer and an organic phase containing a tri-functional acyl-chloride monomer. Once the two phases are contacted, the amine monomer diffuses and partitions across the interface into the organic phase where it reacts with the acyl-chloride [2].

Despite extensive research, the exact mechanisms linking reaction conditions to the final membrane morphology are still not fully understood. Since membrane structure and performance are intimately linked, such mechanistic insight is crucial for better informed membrane fabrication and development [3–5]. For example, the link between surface roughness and permeability of polyamide-based TFC membranes has received much attention, leading to inconclusive results (see Fig. 1a) [6–9]; certainly, these apparent discrepancies may be due to differences in the actual polymerization conditions that manifest in ways other than the roughness. Further, recent studies have shown that the polyamide layer is not homogenous and contains nano-scale voids (see Fig. 1b) that are liquid-filled under operational conditions, and,

most importantly, these voids may be directly connected to the permeate space though holes formed on the back surface of the polyamide film [10–17]. These voids have been shown, theoretically, to produce a positive correlation between roughness and permeability [18]. It is not yet clear what controls membrane roughness and, indeed, why these voids form. It is further unclear whether creating the roughness is indeed the route to increased permeability, as recent studies have shown that high-flux membranes may be fabricated simply by keeping the polyamide layer ultra-thin and smooth [19,20]. Direct measurement of the IP process, its kinetics and link to the resulting membrane morphology has been the subject of several past studies, demonstrating the growth stages and their dependence on reaction conditions (see ref [21] for a brief account). Furthermore, microscopic visualization of IP has recently been conducted, directly illustrating film growth and morphology, while also providing a possible means for performing transport measurements on free-standing films (eliminating the impact of the support structure) [22]. Such methods may hold great promise for better understanding IP.

However, a particular feature of IP appears to have been mostly overlooked - the exothermal nature of the reaction. Since heat is released at a rate proportional to the polymer formed, the interfacial temperature will increase rapidly and it is reasonable to assume that this will affect transport and the mechanics of film formation. Furthermore, should temperatures reach high enough values, it is

* Corresponding author.

E-mail address: ramong@technion.ac.il (G.Z. Ramon).

<https://doi.org/10.1016/j.memsci.2018.09.011>

Received 22 May 2018; Received in revised form 10 July 2018; Accepted 2 September 2018

Available online 04 September 2018

0376-7388/ © 2018 Elsevier B.V. All rights reserved.

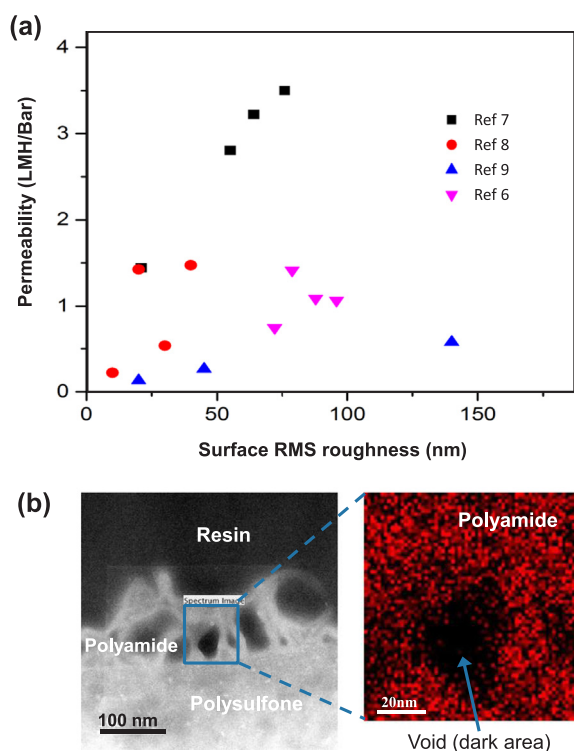


Fig. 1. Morphology of polyamide thin films. (a) Permeability vs. roughness, compiled from the literature (refs [6–9]), illustrating the mixed trends reported. (b) The voids within the polyamide layer of a commercial RO membrane (from ref [17]).

conceivable that interfacial boiling will occur, or some form of dissolved gas release. We propose that, should such bubbling occur at the interface, it might provide an alternative explanation as to the formation of the void structures observed in the polyamide layer. In fact, during a revision of this work, a recent paper has already provided proof of heat-release effects on IP [23]; specifically, the effect of degassing the aqueous phase prior to the reaction was shown to impact the resulting membrane's structure and performance. Also motivated by these questions, and in pursuit of further evidence and understanding of these effects, we performed direct microscopic visualization experiments of interfacial polymerization, conducted using a microfluidic platform. In particular, the temperature field within the microfluidic device was inferred using fluorescence-intensity mapping and image analysis.

2. Experimental

2.1. Materials

Ultra-pure (18.2 mΩ) deionized water was produced using a Milli-Q system (Direct u-3uv, Millipore corp.). For the IP reaction, Trimesoyl-chloride (TMC, Sigma Aldrich no. 182443), m-Phenylenediamine (MPD, Sigma-Aldrich, no. P23954), Piperazine (PIP, Sigma-Aldrich, no. P45907), DiMethyl-Sulfoxide (DMSO, Sigma-Aldrich, no. 276855) and Rhodamine B (Rhb, Sigma-Aldrich, no. 83689) were all used as received. The aqueous reactant solution was prepared by dissolving either

MPD (1.5% w/v) or PIP (2% w/v) along with 0.01 mmol/L Rhb in DI water. The organic reactant solution was prepared by dissolving TMC (0.05% or 0.15%) in isoparG (Gadot Chemical Terminals Ltd.).

2.2. Fabrication of the microfluidic device

The flow channels were fabricated using a standard protocol [24] that included spin coating SU-8 photoresist (Metalchem) on a clean, dry, 4" silicon wafer (Virginia semiconductors), pre-exposure baking, uv-exposure followed by photomask attachment, post-exposure bake and development. The final structure (shown in Fig. 2) provided channel dimensions of 20 μm height and 120 μm width. The mold was then used for fabricating a PDMS-based (SYLGARD 184, Dow Corning) microchannel, and sealed with a thin cover-slide using a corona discharge lab treater (BD-20ACV, ETP).

2.3. Direct microscopic visualization of IP

Interfacial polymerization is an extremely rapid process and commences immediately once the two reactant-carrying solutions are brought into contact. Hence, a careful protocol was required so that experiments could be reproducible. A typical experiment for microscopic imaging of IP involved the following steps (shown schematically in Fig. 2a): (1) flow of the organic phase (TMC solution in isoparG) through the non-splitting outlet; (2) interface stabilization - DI water was introduced into the aqueous channel to form a stable interface with the TMC solution; (3) finally, the fluorescently-labeled aqueous phase (a solution of the amine monomer and Rhb in water) was pumped into the device through the third inlet, replacing the DI water and contacting the organic phase, at which point IP was initiated. Live image acquisition was carried out, at 11 fps, using a laser-scanning confocal microscope (TCS SP8, Leica) with a 25X water-immersion objective (NA = 0.95), through which the channel was monitored, simultaneously, using fluorescent and reflected light channels.

2.4. Measurement of the temperature field

In order to infer the temperature distribution in the microfluidic channel during IP, analysis was performed on the acquired images, exploiting the temperature-sensitive fluorescence of Rhb (for further details of the method, see [25]). Briefly, the method exploits the fact that for a given, constant, Rhb concentration (0.01 mM, in our case) and excitation source power, fluorescence intensity diminishes with temperature at a corresponding rate. This intensity-temperature relation may be calibrated by sequentially quantifying the average pixel intensity in a series of images acquired at different temperatures. In our experiments, we performed the calibration by pumping, into the microfluidic device, a series of solutions at known temperatures held fixed by a heated, temperature-monitored reservoir. For each temperature, a series of images were acquired by the microscope, and the average pixel intensity was provided by the image analysis package of the microscope (LAS, Leica). In the calibration experiments, conditions were maintained identical as the intended IP visualization experiments, in terms of Rhb concentration, laser intensity, and the optics (the microscope objective used), so as to ensure the accurate transfer of the observed intensity-temperature trend. The acquired intensity data is then converted into the known temperatures of the solution at each point (see Fig. 2c) and interpolated into a function used by the image analysis software, in subsequent IP experiments, to map the pixel intensity values to temperatures.

3. Results and discussion

3.1. Effect of reaction conditions on temperature

The temperature time-evolution during typical experiments is shown in Fig. 3, for a range of experimental conditions involving the following variations: reactant flow rates (Fig. 3a); TMC concentration (Fig. 3b); co-solvent addition (Fig. 3c); and amine-monomer (Fig. 3d). In these plots, the temperature is shown at 2 locations - the approximate location of the interface, and 40 μm away from the interface, into the aqueous phase (see illustration in Fig. 2b). All results are summarized in Fig. 4, where the spatial temperature distributions are also shown across the aqueous phase, for all cases considered.

First, the effect of reactant flow-rate was tested, motivated by the fact that large scale membrane production using IP proceeds via a roll-to-roll process, where there is relative motion at the interface during the reaction. Two different flow rates of the aqueous phase were used (5 and 10 $\mu\text{L}/\text{min}$), while the organic phase was kept at a constant flow rate of 5 $\mu\text{L}/\text{min}$.

Temperatures increased rapidly, with more significant changes observed near the interface, reaching temperatures of 75–80 $^{\circ}\text{C}$, with higher temperatures observed at increased flowrate. At the interface, mass transfer of the MPD into the organic phase is crucial, and is a major determining factor for the reaction rate. A higher flowrate of the MPD solution presumably increases the mass transfer and hence the reaction rate, reflected in more intense heat release. We note that the velocity distribution in this co-flow setup is quite complex due to the film formation; initially, the two fluids move at an identical velocity at the interface, dictated by a no-slip condition. However, once a film forms the velocity distribution may change due to immobilization of the interface, resulting in larger gradients and increased heat and mass transfer rates to the interface. This is not to be confused with mass transfer through the interface, which is slowed down by the presence of the forming film. Increasing the TMC concentration also induced higher temperatures (see Fig. 3b), with typical temperatures of $\sim 85^{\circ}\text{C}$ close to the interface, higher than that measured for a lower concentration with a higher flow rate, suggesting that in this case the availability of TMC outweighs the faster transfer of MPD.

Next, DMSO, reported to impact the morphology of the resulting film and increase permeability [26,27], was added to the aqueous solution (see Fig. 3c). The temperature increased substantially within 50 s, reaching values of 70 $^{\circ}\text{C}$ and 80 $^{\circ}\text{C}$ at 40 μm and the interface, respectively, presumably due to the higher rate of MPD transport across the water-oil interface. In the combined case of DMSO addition and high TMC concentration, maximum temperatures reached were $\sim 86^{\circ}\text{C}$ and $\sim 77^{\circ}\text{C}$ at the interface and 40 μm from it, respectively. A combination of faster MPD transport and availability of TMC in the organic phase resulted in the highest rate of film formation and, hence, the greatest amount of heat release.

3.2. Is interfacial polymerization self-limiting?

The kinetics of IP have been discussed in several studies (for example, [2,21,28–30], to mention a few), mostly agreeing upon the dynamics which include an initial, rapid formation of the film followed by a significant slowing down, reaching a so-called self-limiting regime where the polymer film inhibits its own growth. Our own experiments also exhibit a distinctive 2-stage evolution of the temperature (the point of transition is marked by dashed vertical lines in Fig. 3a-c), presumably a reflection of film thickness, which is the usual explanation, but possibly also an indication of film integrity, where a contiguous film begins to form and thus further polymerization is slowed down significantly. A transition is observed 5–10 s into the reaction (with some small uncertainty during the initial seconds of the experiment), in general

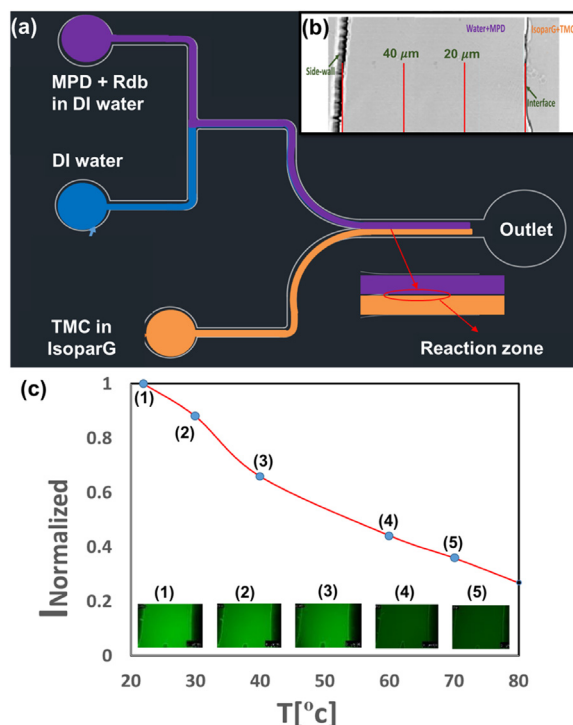


Fig. 2. Experimental system. (a) schematic of the flow cell, with the different inlets for the reactants and the reaction zone at the interface between the water and oil phases. (b) Bright-field image of the reaction zone and the flow domain of the aqueous stream. (c) Sequential fluorescence imaging at increasing temperatures, conducted in order to generate the calibration curve – fluorescence intensity vs. temperature, scaled against the nominal value at 22 degrees C. Images at bottom correspond with demarcated points on the curve.

agreement with past observation, although it appears that the slowing down is not so dramatic. The main difference between past studies and the current one is the continuous flow of monomers vs. the static conditions commonly applied in lab-scale formation of IP membranes. In the current setup, the formed films continued to grow, albeit slower, reaching thicknesses far greater (by several orders of magnitude) than is commonly observed for TFC membranes, and suggesting that the reaction is not as self-limiting as previously observed but, rather, is mostly limited by a continuous, rapid supply of monomers – particularly the amine. Another difference in our setup is the lack of the porous support used when fabricating IP-based membranes. Recent studies have shown that support-free IP results in different morphologies, compared with supported IP [31,32], but mostly in the ability to create thin, smooth films as well as the independent control over the support used, which has been shown to significantly impact the overall permeability [33]. If, indeed, the main difference is the flow and supply of monomers to the interface, then this effect could be manifested in supported TFC fabrication via a limited amount of the amine monomer or hinderance to its transport, affected by the properties of the support membrane, for example its porosity and hydrophilicity [31,34].

The final set of experiments tested the effect of the amine monomer, with PIP replacing MPD (see Fig. 3d) and reflecting the difference between RO and NF membranes. These experiments exhibited quite different characteristics. First, the temperature rise was significantly slower and the interfacial temperature was at least a factor of 2 smaller than observed for the MPD system. Second, no transition in heat release rate is apparent. This is presumably due to extremely fast kinetics which possibly creates a truly contiguous film, producing self-limiting conditions that rapidly slow down further polymerization.

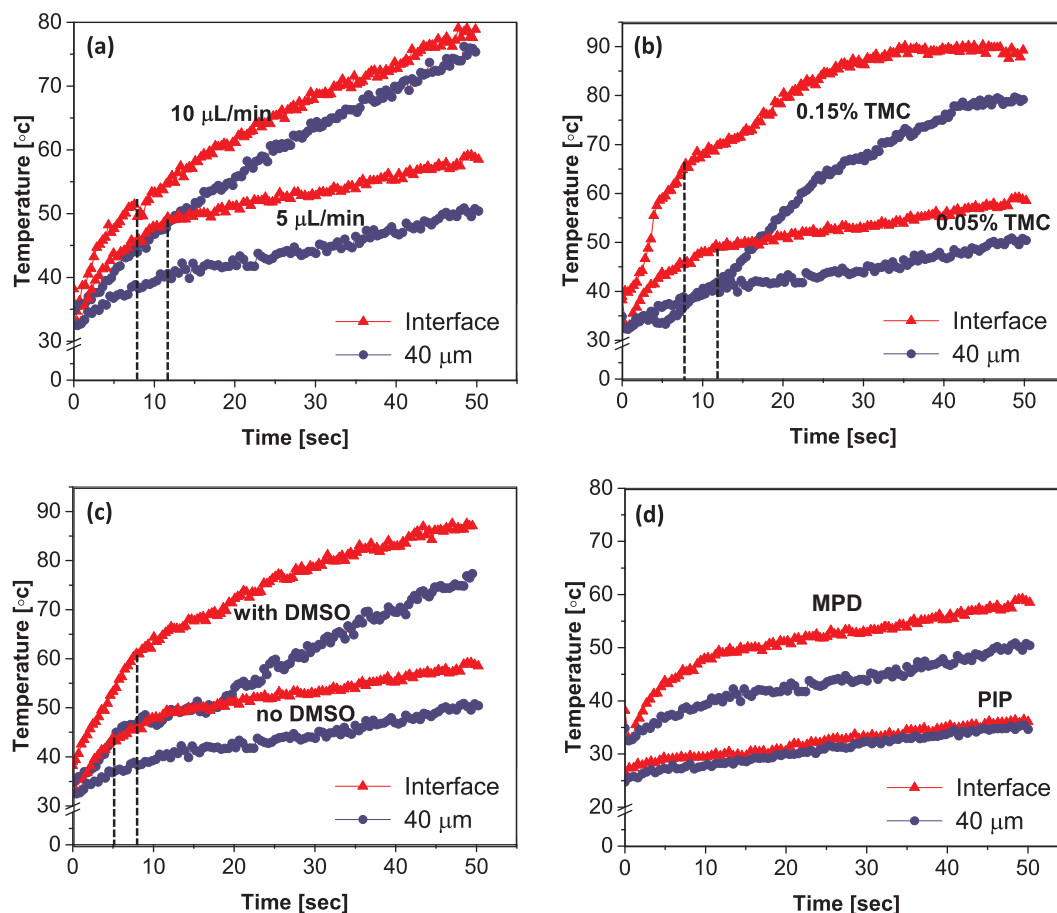


Fig. 3. Time evolution of the temperature at two locations in the microfluidic channel: close to the interface and $40\ \mu\text{m}$ into the aqueous phase, under different experimental conditions: a) Flowrates of the aqueous phase. b) Organic phase monomer concentration. c) Addition of co-solvent. d) Variation of the amine monomer. Dashed vertical lines mark the observed transition from presumed fast initial film formation to the slowing down stage (not marked on figure (d) since this transition was not observed for the PIP system).

Ultimately, formulations that encourage faster mass transfer seem to produce similar trends in terms of the temperature time evolution (reflecting the rate of polymer formation), the magnitude of interfacial temperature as well as the temperature distribution within the channel (see Fig. 4). The insensitivity of the temperature distribution to the flowrate (at long times) is striking particularly at the increased flow rate, suggesting that heat transfer occurs primarily through conduction. Note that this refers to the temperature profiles across the channel, not the value of the temperature, which changed significantly when the base formulation was tested under two different flowrates. The 2D-confined geometry does not seem to play a significant role here, since the thermal diffusivity of glass is ~ 4 times higher than water and should produce, if anything, a more efficient heat sink than would be expected in a truly 3D environment.

3.3. A possible correlation between morphology and heat release

A main motivation for examining the heat release during the reaction was the question to what extent does this impact the film morphology and, hence, transport? While our reported results, shown in Fig. 5c-h, may still be viewed as preliminary, we nevertheless make two careful observations. First, different conditions varied the resulting morphologies. A particular feature, which served as our initial working hypothesis, was the formation of what appear to be voids within the polyamide layer. The temperatures measured approach the boiling temperature of water, let alone some common solvents used for IP (e.g., Hexane), suggesting that such interfacial boiling or soluble gas release is highly likely and worthy of further scrutiny – the latter effect has already been reported recently [21]. A point to consider is that in the reported study by Ma et al. [21] the organic solvent used was Hexane, which, according to our results, may indeed boil and contribute to the

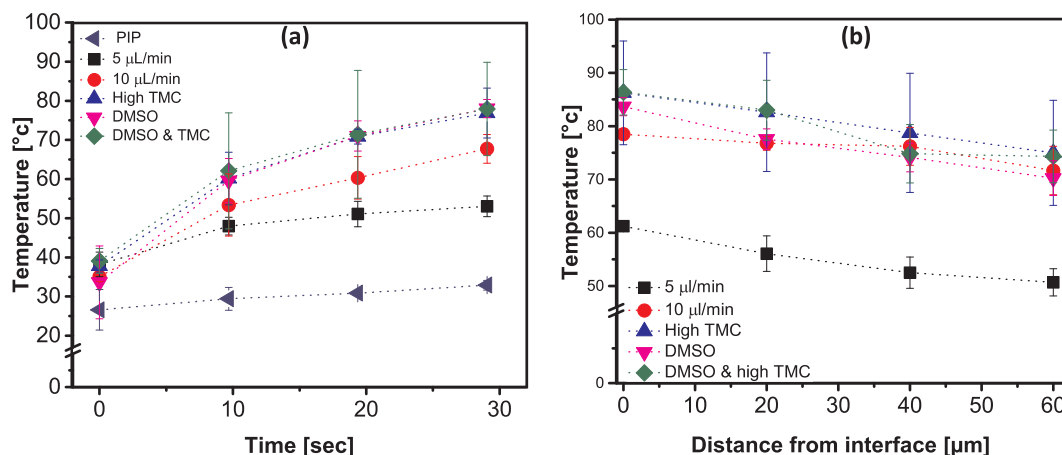


Fig. 4. Summary of experimental results. a) Time evolution of the temperature close to the interface, for all experimental conditions. b) Spatial temperature distribution within the aqueous phase. Measurements are shown at $t = 60$ s. The error bars represent the standard deviation from the mean, for up to 10 repetitions of an experiment (but no fewer than 3).

possible void formation through the proposed nanobubble mechanism.

Second, and perhaps surprising, some of the images obtained in our experiments bear a striking resemblance to reported morphologies – despite the enormous difference in spatial scales, which are on the order of microns in our case and tens to hundreds of nanometers in TFC's. Such a similitude may be of profound impact as it would allow optical, in-situ methods such as reported herein, to be used for making preliminary assessments of film morphologies obtained under different conditions. Future refinement of the system can include a geometry capable of supporting post-polymerization procedures so that the self-supporting films can be characterized for their transport properties and extracted for electron microscopy analysis or other advanced characterization. Such a microfluidic-based system could be used for a massively parallel exploration of chemistries, additives and conditions, providing a rapid prototyping of potential materials, using small samples and short time scales, and ultimately leading to better informed membrane design. Such implementation would have to rely, first and foremost, on proof that the tested chemistry has the potential to function as a good separation barrier and future development of a microfluidic platform capable of measuring the transport properties of the resulting polymeric film.

4. Concluding remarks

Motivated by questions related to the heat release during IP and its effect on the resulting polyamide thin film, a microfluidic methodology was developed and demonstrated for in-situ, optics-based temperature measurement within the reaction zone. Our results demonstrate, for the first time, the magnitude of the temperature generated near the reaction zone, and how it is affected by some variations of the reaction conditions. The largest impact is found to be the flow rate of the aqueous phase, organic phase monomer concentration and choice of amine monomer. The addition of a co-solvent that presumably increases the

partitioning of the amine monomer, increased the reaction rate and the temperature. A striking result of this study is that temperatures near the reaction zone can exceed the boiling point of some solvents used in IP, suggesting that soluble gas release and possibly interfacial boiling may occur and perhaps contribute to the formation of voids within the polyamide film as it forms. In our experiments, we used a non-boiling solvent and voids still appeared to form, presumably due to release of soluble gases. However, we cannot completely rule out the possible boiling of water at the interface, where temperatures may be higher, on the nano-scale, than those actually measured (likely at a distance of several microns from the reaction zone).

Furthermore, bright-field images of the interface indicated formation of thick films, orders of magnitudes larger than found in practice, suggesting that the film formation is not severely self-limiting (there may be some degree of slowing-down, as manifested by the temperature increase rate) and will continue growing as long as there is supply of reactants to the interface. In IP performed on porous supports, this suggests that the support plays a role in dictating the film formation by determining the availability of amine – this may be through the solution contained within the pores of the support, but also a residual aqueous film on the solid support surface, dictated, to a large extent, by the hydrophilicity of the membrane support material. In contrast, the PIP monomer exhibited slower growth and significantly lower heat release.

Finally, images of the formed films bear some striking qualitative resemblance to TEM images of 'real' polyamide films void formation. If there is indeed some scale-similitude, then optical-based systems such as the one reported herein may open an additional path to studying polyamide morphologies, offering a possibility to perform rapid assessment of materials and conditions using small material quantities. Future work may use this platform to further study the behavior of new or known formulations and add an additional layer of insight to their characterization.

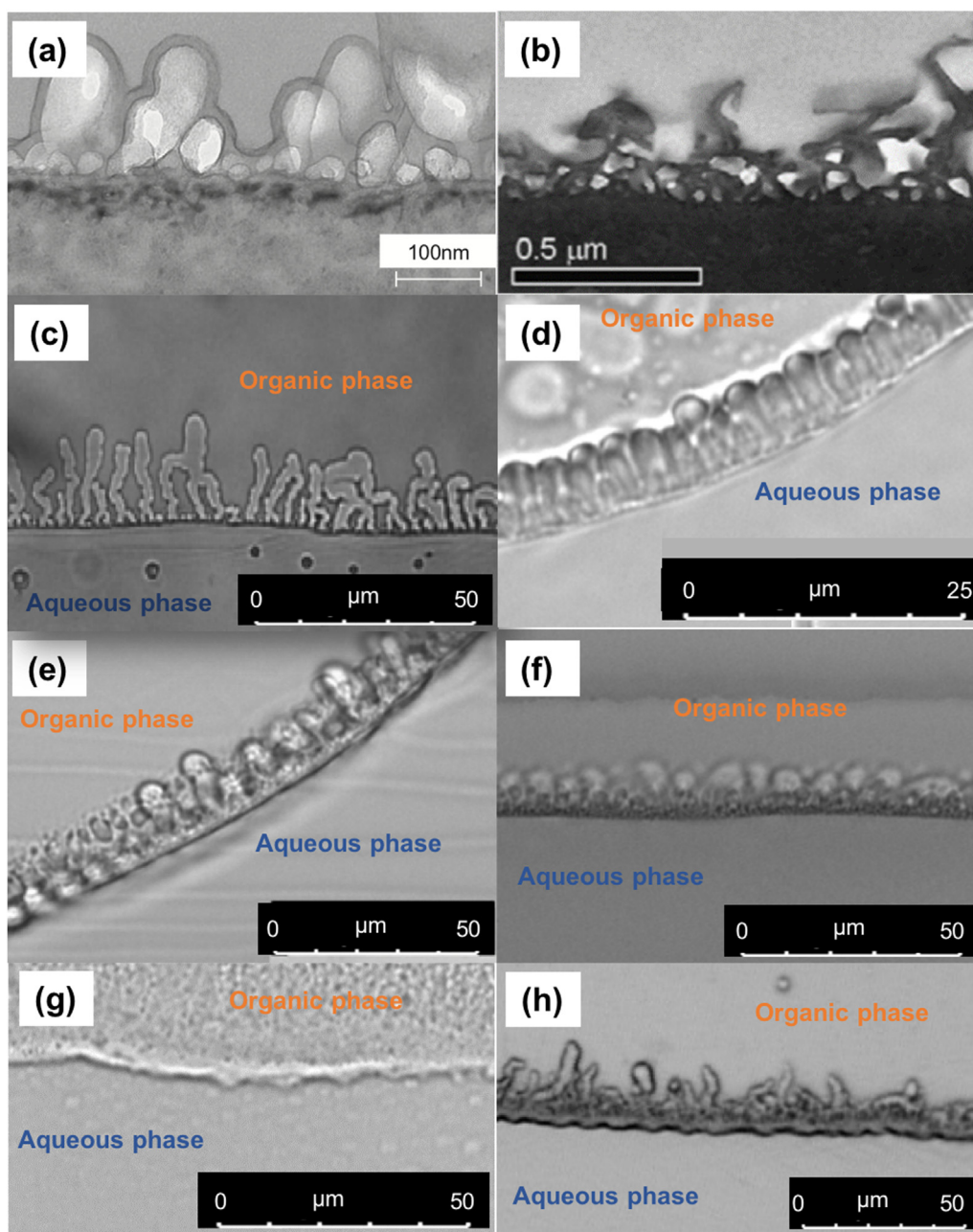


Fig. 5. Polyamide film morphologies reported in the literature (a-b) and visualized in the current study (c-f), obtained after 60 s: (a-b) TEM sections reported in the literature [13,16]. (c) 1.5% MPD, 0.05% TMC. (d) 1.5% MPD, 0.15% TMC. (e) 1.5% MPD, 0.05% TMC and 0.25% DMSO. (f) 1.5% MPD, 0.15% TMC and 0.25% DMSO. (g) 2% PIP, 0.05% TMC. (h) conditions identical to (c), after 5 min of polymerization.

Appendix A. Supporting information

Supplementary data associated with this article can be found in the online version at [doi:10.1016/j.memsci.2018.09.011](https://doi.org/10.1016/j.memsci.2018.09.011).

References

- [1] M. Elimelech, W.A. Phillip, The future of seawater desalination: energy, technology, and the environment, *Science* (80-). 333 (2011) 712–717, <https://doi.org/10.1126/science.1200488>.
- [2] V. Freger, Kinetics of film formation by interfacial polycondensation, *Langmuir* 21 (2005) 1884–1894, <https://doi.org/10.1021/la048085v>.
- [3] M.J.T. Raaijmakers, N.E. Benes, Current trends in interfacial polymerization chemistry, *Prog. Polym. Sci.* 63 (2016) 86–142, <https://doi.org/10.1016/j.progpolymsci.2016.06.004>.
- [4] B.S. Lalia, V. Kochkodan, R. Hashaikeh, N. Hilal, A review on membrane fabrication: structure, properties and performance relationship, *Desalination* 326 (2013) 77–95, <https://doi.org/10.1016/j.desal.2013.06.016>.
- [5] S. Hermans, R. Bernstein, A. Volodin, I.F.J. Vankelecom, Study of synthesis parameters and active layer morphology of interfacially polymerized polyamide-polysulfone membranes, *React. Funct. Polym.* 86 (2015) 199–208, <https://doi.org/10.1016/j.reactfunctpolym.2014.09.013>.
- [6] A.K. Ghosh, B.-H. Jeong, X. Huang, E.M.V. Hoek, Impacts of reaction and curing conditions on polyamide composite reverse osmosis membrane properties, *J. Membr. Sci.* 311 (2008) 34–45, <https://doi.org/10.1016/j.memsci.2007.11.038>.
- [7] M. Hirose, H. Ito, Y. Kamiyama, Effect of skin layer surface structures on the flux behaviour of RO membranes, *J. Membr. Sci.* 121 (1996) 209–215, [https://doi.org/10.1016/S0376-7388\(96\)00181-0](https://doi.org/10.1016/S0376-7388(96)00181-0).
- [8] S. Al-Jeshi, A. Neville, An investigation into the relationship between flux and roughness on RO membranes using scanning probe microscopy, *Desalination* 189 (2006) 221–228, <https://doi.org/10.1016/j.desal.2005.08.001>.
- [9] S.Y. Kwak, S.G. Jung, Y.S. Yoon, D.W. Ihm, Details of surface features in aromatic polyamide reverse osmosis membranes characterized by scanning electron and atomic force microscopy, *J. Polym. Sci. Part B Polym. Phys.* 37 (1999) 1429–1440, [https://doi.org/10.1002/\(SICI\)1099-0488\(19990701\)37:13<1429::AID-POLB9>3.0.CO;2-B](https://doi.org/10.1002/(SICI)1099-0488(19990701)37:13<1429::AID-POLB9>3.0.CO;2-B).

- [10] H. Yan, X. Miao, J. Xu, G. Pan, Y. Zhang, Y. Shi, M. Guo, Y. Liu, The porous structure of the fully-aromatic polyamide film in reverse osmosis membranes, *J. Membr. Sci.* 475 (2015) 504–510, <https://doi.org/10.1016/j.memsci.2014.10.052>.
- [11] T. Kamada, T. Ohara, T. Shintani, T. Tsuru, Optimizing the preparation of multi-layered polyamide membrane via the addition of a co-solvent, *J. Membr. Sci.* 453 (2014) 489–497, <https://doi.org/10.1016/j.memsci.2013.11.028>.
- [12] S. Zhu, S. Zhao, Z. Wang, X. Tian, M. Shi, J. Wang, S. Wang, Improved performance of polyamide thin-film composite nanofiltration membrane by using poly-etersulfone/polyaniline membrane as the substrate, *J. Membr. Sci.* 493 (2015) 263–274, <https://doi.org/10.1016/j.memsci.2015.07.013>.
- [13] T. Kamada, T. Ohara, T. Shintani, T. Tsuru, Controlled surface morphology of polyamide membranes via the addition of co-solvent for improved permeate flux, *J. Membr. Sci.* 467 (2014) 303–312, <https://doi.org/10.1016/j.memsci.2014.03.072>.
- [14] Y. Li, M.M. Kłowski, C.M. McGilvery, A.E. Porter, A.G. Livingston, J.T. Cabral, Probing flow activity in polyamide layer of reverse osmosis membrane with nanoparticle tracers, *J. Membr. Sci.* 534 (2017) 9–17, <https://doi.org/10.1016/j.memsci.2017.04.005>.
- [15] M.M. Kłowski, C.M. McGilvery, Y. Li, P. Abellan, Q. Ramasse, J.T. Cabral, A.G. Livingston, A.E. Porter, Micro-to nano-scale characterisation of polyamide structures of the SW30HR RO membrane using advanced electron microscopy and stain tracers, *J. Membr. Sci.* 520 (2016) 465–476, <https://doi.org/10.1016/j.memsci.2016.07.063>.
- [16] F. Pacheco, R. Sougrat, M. Reinhard, J.O. Leckie, I. Pinnau, 3D visualization of the internal nanostructure of polyamide thin films in RO membranes, *J. Membr. Sci.* 501 (2015) 33–44, <https://doi.org/10.1016/j.memsci.2015.10.061>.
- [17] L. Lin, R. Lopez, G.Z. Ramon, O. Coronell, Investigating the void structure of the polyamide active layers of thin-film composite membranes, *J. Membr. Sci.* 497 (2016), <https://doi.org/10.1016/j.memsci.2015.09.020>.
- [18] M.C.Y. Wong, L. Lin, O. Coronell, E.M.V. Hoek, G.Z. Ramon, Impact of liquid-filled voids within the active layer on transport through thin-film composite membranes, *J. Membr. Sci.* 500 (2016) 124–135, <https://doi.org/10.1016/j.memsci.2015.11.033>.
- [19] S. Karan, Z. Jiang, A.G. Livingston, Sub-10 nm polyamide nanofilms with ultrafast solvent transport for molecular separation, *Science* (80) 348 (2015) 1347–1351, <https://doi.org/10.1126/science.aaa5058>.
- [20] B. Khorshidi, T. Thundat, B.A. Fleck, M. Sadzadeh, A novel approach toward fabrication of high performance thin film composite polyamide membranes, *Sci. Rep.* 6 (2016) 22069, <https://doi.org/10.1038/srep22069>.
- [21] T.D. Matthews, H. Yan, D.G. Cahill, O. Coronell, B.J. Mariñas, Growth dynamics of interfacially polymerized polyamide layers by diffuse reflectance spectroscopy and Rutherford backscattering spectrometry, *J. Membr. Sci.* 429 (2013) 71–80, <https://doi.org/10.1016/j.memsci.2012.11.040>.
- [22] Y. Zhang, N.E. Benes, R.G.H. Lammertink, Visualization and characterization of interfacial polymerization layer formation, *Lab Chip* 15 (2015) 575–580, <https://doi.org/10.1039/C4LC01046A>.
- [23] X.H. Ma, Z.K. Yao, Z. Yang, H. Guo, Z.L. Xu, C.Y. Tang, M. Elimelech, Nanofoaming of polyamide desalination membranes to tune permeability and selectivity, *Environ. Sci. Technol. Lett.* 5 (2018) 123–130, <https://doi.org/10.1021/acs.estlett.8b00016>.
- [24] Y. Xia, G.M. Whitesides, Soft lithography, *Annu. Rev. Mater. Sci.* 28 (1998) 153–184, <https://doi.org/10.1146/annurev.matsci.28.1.153>.
- [25] D. Ross, M. Gaitan, L.E. Locascio, Temperature measurement in microfluidic systems using a temperature-dependent fluorescent dye, *Anal. Chem.* 73 (2001) 4117–4123, <https://doi.org/10.1021/ac010370l>.
- [26] S.Y. Kwak, S.G. Jung, S.H. Kim, Structure-motion-performance relationship of flux-enhanced reverse osmosis (RO) membranes composed of aromatic polyamide thin films, *Environ. Sci. Technol.* (2001), <https://doi.org/10.1021/es010630g>.
- [27] S.H. Kim, S.Y. Kwak, T. Suzuki, Positron annihilation spectroscopic evidence to demonstrate the flux-enhancement mechanism in morphology-controlled thin-film-composite (TFC) membrane, *Environ. Sci. Technol.* (2005), <https://doi.org/10.1021/es049453k>.
- [28] G.Y. Chai, W.B. Krantz, Formation and characterization of polyamide membranes via interfacial polymerization, *J. Membr. Sci.* 93 (1994) 175–192, [https://doi.org/10.1016/0376-7388\(94\)80006-5](https://doi.org/10.1016/0376-7388(94)80006-5).
- [29] V. Freger, Nanoscale heterogeneity of polyamide membranes formed by interfacial polymerization, *Langmuir* 19 (2003) 4791–4797, <https://doi.org/10.1021/la020920q>.
- [30] A. Nowbahar, V. Mansard, J.M. Mecca, M. Paul, T. Arrowood, T.M. Squires, Measuring interfacial polymerization kinetics using microfluidic interferometry, *J. Am. Chem. Soc.* 140 (2018) 3173–3176, <https://doi.org/10.1021/jacs.7b12121>.
- [31] S.J. Park, W. Choi, S.E. Nam, S. Hong, J.S. Lee, J.H. Lee, Fabrication of polyamide thin film composite reverse osmosis membranes via support-free interfacial polymerization, *J. Membr. Sci.* 526 (2017) 52–59, <https://doi.org/10.1016/j.memsci.2016.12.027>.
- [32] Z. Jiang, S. Karan, A.G. Livingston, Water transport through ultrathin polyamide nanofilms used for reverse osmosis, *Adv. Mater.* 30 (2018) 1–7, <https://doi.org/10.1002/adma.201705973>.
- [33] G.Z. Ramon, M.C.Y. Wong, E.M.V. Hoek, Transport through composite membrane, Part 1: is there an optimal support membrane? *J. Membr. Sci.* 415–416 (2012) 298–305, <https://doi.org/10.1016/j.memsci.2012.05.013>.
- [34] A.K. Ghosh, E.M.V. Hoek, Impacts of support membrane structure and chemistry on polyamide-polysulfone interfacial composite membranes, *J. Membr. Sci.* 336 (2009) 140–148, <https://doi.org/10.1016/j.memsci.2009.03.024>.